ACS Energy LETTERS

Open Access

http://pubs.acs.org/journal/aelccp

Revisiting Active Site Quantification in CO_2 Electroreduction: The Case for CO Displacement

Yuxiang Zhou,[#] Benjamin Bowers,[#] Alexander Bagger, Guangmeimei Yang, Ludmilla Steier,* Mary P. Ryan,* and Ifan E. L. Stephens*

Cite This: *ACS Energy Lett.* 2025, 10, 4324−4331

Read Online

ACCESS | Metrics & More | Article Recommendations | Supporting Information

ABSTRACT: The selectivity and geometric current density of copper-based electrodes for electrochemical CO_2 reduction (CO_2RR) have been significantly improved, yet research is striving to improve the intrinsic activity of these materials. The accurate quantification of active sites is vital to benchmark the intrinsic activity of the catalysts for electrochemical CO_2 reduction to facilitate activity improvements. Herein, we propose a method to determine the active sites using CO displacement in potassium phosphate buffer at 10 °C. Comparing this method with the electrochemical surface area (ECSA), measured by double-layer capacitance, the most used technique in this field, we demonstrate that CO displacement provides a much more accurate quantification of the number of active sites. By normalizing current density vs the CO displacement active sites, we find electropolished copper foil has the highest intrinsic activity towards CO_2RR. We also reveal there is a clear relationship between surface roughness and chained products.

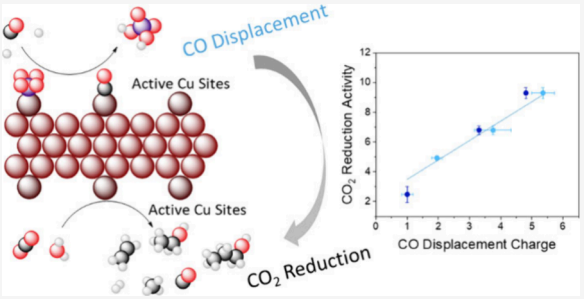

Electrochemical CO_2 reduction (CO_2RR) provides a strategy to achieve low carbon fuels and chemical feedstock. To date, copper (Cu) is the only monometallic catalyst that can yield, high value, C_{2+} molecules at high faradaic efficiencies (FE) due to its suitable binding energy towards key intermediates *CO and *H.[1] Significant strides have been made in altering the selectivity of these Cu-based catalysts by tuning the nanostructure,[2−5] composition,[6−16] utilizing facet effects[17,18] and electrolyte effects.[19−24] As a result, the FE towards valuable products ethylene and ethanol have been reported to reach up to 87%[25] and 52%[26] respectively.

Such highly selective Cu-based CO_2RR catalysts still suffer from low intrinsic activity and poor stability. To the best of our knowledge, electropolished polycrystalline Cu still shows the highest CO_2RR intrinsic activity, despite forming 16 different CO_2RR products.[27−29] Moreover, Cu tends to reconstruct and degrade under reaction conditions.[30−33] Therefore, to scale up this reaction, a catalyst with similar intrinsic CO_2RR activity to polycrystalline Cu, but much better selectivity and long-term stability must be found.[34−36] The discovery of such a catalyst would be strongly accelerated if we had improved our understanding of the factors controlling CO_2 reduction and in particular improved methods to measure the intrinsic catalytic activity.

An accurate estimation of intrinsic activity is crucial to benchmark a catalyst performance and understand the CO_2RR kinetics and, in turn, the mechanism. In electrocatalysis, intrinsic activity of a catalyst is and can only be evaluated by the turnover frequency (TOF), the number of moles of reactant converted per active site per unit time.[29] In practice, partial current density normalised by the electrochemical active surface area (ECSA) is often used to represent the TOF. Double layer capacitance (C_{dl}) is the most widely used method for measuring ECSA of Cu-based materials.[37] C_{dl} consists of cyclic voltammetry (CV) under different scan rates in the potential window without the Faradaic process. The buildup of charge and discharge is measured and related to the capacitance.[38] However, discrepancies often arise between the ECSA measured by double layer capacitance and other methods, like Pb-under potential deposition (UPD).[37,39] Additionally, the adsorbed species during C_{dl} measurement

Received: May 30, 2025
Revised: July 28, 2025
Accepted: August 7, 2025
Published: August 12, 2025

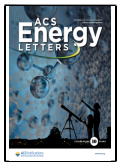

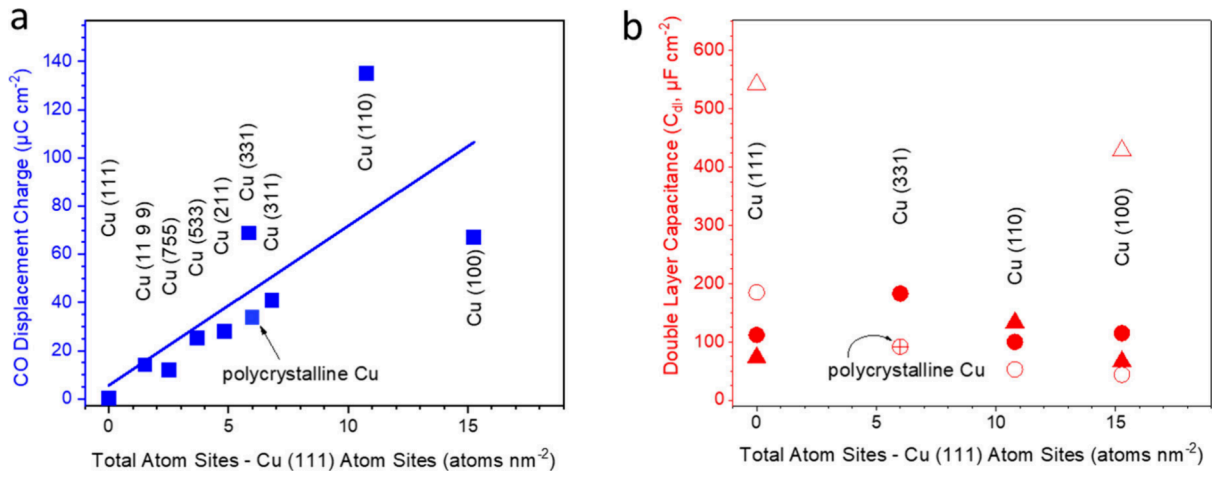

Figure 1. Comparison of the facet dependence of the (a) CO displacement charges in pH 6.8, 0.2 M phosphate buffer, and (b) double layer capacitances. The X axis converts the Cu facets to the densities of Cu atoms ((111) not included). The CVs used for calculating the double layer capacitances and CO displacement charges can be found in Figures S1 and S3, respectively. Data was obtained from Koga, Hori, Hochfilzer, Tiwari, Engstfeld, Raaijman, Le Duff, Schouten et al.[43,44,56,58−64].

remains unclear.[40] Even on Pt single crystals, a much more well understood surface, the double layer capacitance can easily change by a factor of 2 between different facets, and there are huge discrepancies on the surface area measured by different methods, including CO stripping, H-UPD, Pb-UPD, and double layer capacitance.[41] Single crystal studies on Cu showed similar issues (Figure S1). Furthermore, there are questions whether non-faradaic capacitance can be related to CO_2RR active sites, at reaction potential,[42] as the sites that are active for double layer capacitance measurement might not be also active for CO_2RR. Therefore, a new method for measuring the CO_2RR active sites on Cu-based materials is required which allows performance to be more accurately related to intrinsic activity.

In the 1990s, Hori et al. first showed that a charge transfer occurs on a Cu electrode under cathodic conditions in phosphate buffer with CO present. A reproducible and sharp peak at around −0.7 V vs NHE appeared in the CV scan (Figure S2a).[43] The in situ Fourier-transform infrared spectroscopy (FTIR) studies indicated that this charge transfer process involved the exchange between CO and adsorbed phosphates (HPO_4^{2-} and PO_4^{3-}) on the Cu surface, which can be termed as the CO displacement reaction.[44,45] Such process was strongly dependent on the electrolyte pH (Figure S2b). Phosphoric acid is a tritropic acid with pK_a values of 2.15, 7.21, and 12.35.[46] In pH 2.15 to 7.21 aqueous solution, the most common CO_2RR pH range, CO displacement reactions can be described by the following two equations.

$$^*HPO_4 + H^+ + 2e^- + CO \leftrightarrow H_2PO_4^- + {}^*CO \quad (1)$$

$$^*PO_4 + 2H^+ + 3e^- + CO \leftrightarrow H_2PO_4^- + {}^*CO \quad (2)$$

where * denotes adsorbed species. Hori and co-workers' electrochemistry data showed that the CO displacement peak shifts around 37 mV pH^{-1} in the neutral pH region (Figure S2b),[44] indicating that eq 2 is the main reaction occurring in pH 2.15 to 7.21 phosphate buffer. A similar trend and pH-dependent voltage slope was also observed by Sebastián-Pascual et al.[46]

Hori's work additionally showed that the charge transferred during the CO displacement process is independent of CV scan rate, providing the possibility of using this method to estimate the amount of CO_2RR active sites of Cu-based materials.[45] Additionally, numerous spectroscopic studies,[47−51] and DFT calculations coupled with principal component analysis based on the Hori's[52,53] CO_2 reduction results of various Cu single crystals conducted by Bagger et al.[1,54,55] provide strong evidence that *CO binding energy serves as an effective descriptor for CO_2 reduction towards more reduced products beyond CO - typically the desired products on Cu surfaces. Therefore, compared with the conventional double layer capacitance method, CO displacement should allow a better quantification of the CO_2RR active sites on Cu-based materials for >2e⁻ products, under the assumption of no surface reconstruction.

Hori et al. further found a potential-temperature dependence for CO displacement (Figure S2c). Decreasing temperature can enhance the solubility of CO in electrolyte and suppress the hydrogen evolution reaction (HER) and CO reduction reaction (CORR),[45] allowing a visible peak of the displacement reaction in a CV. Single crystal studies showed both the CO displacement charge and double layer capacitance has a crystalline facet dependence (Figure S3). For double layer capacitance, even on the same facets and under the same electrolyte, significantly different values (C_{dl}, μF cm^{-2}) were obtained by different groups, as demonstrated by Figure 1 a. Previous studies from Engstfeld et al. also showed that different polishing and cleaning methods on polycrystalline Cu could also lead to different CVs, resulting in varying double layer capacitances.[56] For CO displacement, Hori et al. showed that on Cu (111), CO does not displace phosphate, i.e., the displacement charge is zero. On the other hand, there is a linear correlation between the displacement charge and the number of all other atoms, including Cu(100) and step sites, as shown in Figure 1b. This correlation is consistent with multiple groups' observations on Cu single crystals that closely packed Cu(111) is inactive towards CO_2RR (presumably because CO does not adsorb strongly onto it) while the remaining sites contribute towards CO_2RR activity.[52,55,57] However, it has thus far been unclear how these observations on planar extended surfaces translate directly to technologically relevant nanostructured materials.

https://doi.org/10.1021/acsenergylett.5c01642
ACS Energy Lett. 2025, 10, 4324−4331

Herein, we explore the usage of the CO displacement charge as a probe of the number of CO_2RR active sites on Cu-based nanostructured catalysts, under the assumption of no surface reconstruction; on this basis, we are able to provide a more accurate measure of the intrinsic catalytic activity of Cu-based materials.

We aimed to replicate Hori's CO displacement experiments in 0.2 M phosphate buffer electrolyte under different temperatures and pH (Figure S4). The experiments were undertaken in an H-cell configuration on an electropolished copper foil electrode; our XRD experiments showed that this foil had a preferential orientation in the (200) plane. The copper foil electrode was electropolished at 2.1 V in 85% H_3PO_4 for 5 min. The anolyte was cooled in a jacket beaker and circulated into the cell at 5 mL min^{-1} using a peristaltic pump (Figures S5 and S6). A sustainion anion exchange membrane (AEM) was used to separate the anolyte and catholyte, limiting electrolyte cross over, but allowing heat transfer to cool down the catholyte. The temperature was monitored by an alcohol thermometer. The reaction was completed in 0.2 M K_2HPO_4 (pH 9) and 0.1 M K_2HPO_4 + 0.1 M KH_2PO_4 (pH 6.8), at temperatures of 10, 16 and 20 °C. The copper foil electrode was prereduced in Ar (at −226 μA cm^{-2}) until the cell potential increased to around −0.9 V and CVs were swept between −0.5 and −1.1 V vs NHE until a consistent current response formed.[44] CO was introduced with the electrode held at −0.5 V vs NHE to form the metallic state of copper and the cell was purged for 30 min before repeating the same CV scans as in Ar (see the Supporting Information for a more detailed methodology).

Our results showed a similar trend to Hori et al., with CO displacement peak size decreasing with increasing temperature (Hori et al.[43] in Figure S2c and this work in Figure S4) and a pH dependence of 32 mV pH^{-1} was observed compared to the value of 37 mV pH^{-1} described by Hori et al.[43] (Figure S4c). We attribute the lower value of the CO displacement charge across the pH and temperature range in our experiments to differences in the copper foil, electropolishing method, and cells used.[43,45,65]

To assess double layer capacitance and CO displacement for quantifying CO_2RR active sites, an electropolished copper foil was pretreated by three different ways to change the surface roughness; electropolishing (Figures 2a and S7a), anodization (Figures 2b,c and S7b,c), and electrodeposition (Figure 2d and S7d). The different methods for nanostructuring occurred on different pieces of the same (200) preferred orientation copper foil (Figure 2). All copper foil electrodes were mechanically polished and electropolished before pretreatment. Anodized samples (Figure S7b,c) were prepared by applying 8 mA cm^{-2} to the working electrode Cu foil in 3 M KOH to form $Cu(OH)_2$ nanowires.[66,67] This was followed by electrochemical reduction at −226 μA cm^{-2} in 0.1 M $KHCO_3$. The potential for the anodization increased as nanowires formed. We curtailed the potential to a maximum of 2 V vs Ag/AgCl to avoid delamination of the $Cu(OH)_2$ nanowires. Just before this point, the surface was "fully anodized". After 1.5 min of anodization and then reduction (Figure 2b), the surface was roughened but had not yet formed the dendritic structure in Figure 2c named "fully anodized". Copper "flakes" decorated the surface, linked to the dissolution of copper and redeposition,[68] which was the proposed process for the dendrite formation.[66] The electrodeposited samples were prepared by applying −0.2 mA cm^{-2} to the working electrode

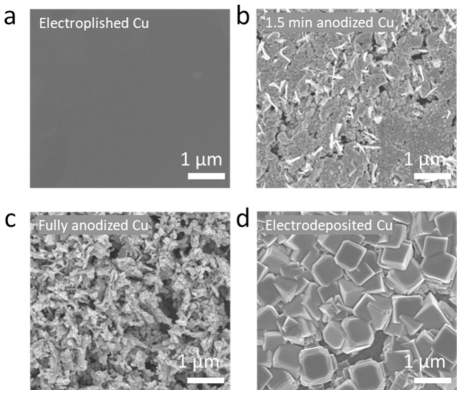

Figure 2. SEM images of the 4 pretreated electrodes. (a) Polycrystalline Cu electropolished at 2.1 V in 85% H_3PO_4 for 5 min; (b) 1.5 min anodized Cu at 8 mA cm^{-2} in 3 M KOH, followed by the in situ reduction at −226 μA cm^{-2} in 0.1 M $KHCO_3$; (c) Fully anodized Cu at 8 mA cm^{-2} in 3 M KOH followed by the same in situ reduction process; (d) Electrodeposited Cu in a $CuSO_4$, lactic acid and KOH solution for 3 C of charge passed followed by the same in situ reduction process. SEM images were taken on a Zeiss Sigma, with 5 kV as the acceleration energy of the incident electron beam.

Cu foil in a $CuSO_4$, lactic acid and KOH solution, until a total of 3 C charge passed[69] (Figure S7d). A cubic structure was formed. As before, this was followed by an electrochemical reduction After 3 C of charge passed, the cubes completely covered the copper foil surface.

CO displacement CVs were taken with an H-cell in pH 6.8 buffer (0.1 M K_2HPO_4 + 0.1 M KH_2PO_4), matching the pH for CO_2RR (0.1 M $KHCO_3$), at 10 °C. As previously discussed, the CO displacement experiment conducted at lower temperature (10 °C) to minimize the influence of HER current, improving the signal to noise ratio, but still does not veer too far from the temperature at which we conduct our catalytic tests. This condition was used for subsequent data analysis and comparison to the CO_2RR activity. We note that the CO_2RR is typically performed at room temperature (approximately 20 °C), and in electrolyte with different anion type (HCO_3^-) and cation (K^+) concentrations. The CO adsorption sites on Cu surfaces are assumed not to be significantly affected by this ∼10 °C temperature and electrolyte-type difference. The redox peaks were caused by the displacement between surface adsorbed CO and phosphate ions. The peak was integrated and highlighted by a blue fill (Figures 3 and S8) (see Supporting Information for further information). This peak was at its most sharp for the electropolished sample (Figure 3a,c), which has a strong preferential orientation along the (200) plane (Figure S9). The more diffuse peaks were observed on the rougher samples, which have a greater contribution in the GIXRD from planes parallel to (111) and (110) (Figure S9), consistent with the corresponding single crystal surfaces probed by Hori et al.[43,45] The potential for displacement was similar on the electropolished and anodized samples yet occurs at a slightly more negative potential for the electrodeposited sample (Figures 3 and S8). The peak was reproducible for many cycles and absent under Ar (Figures 3a, S10, and S11). Potential hold measurements, where a chronoamperometry measurement was held at a potential just more negative than the displacement peak with and without CO, further confirmed that this current resulted from the CO displacement reaction (Figures 3c and

https://doi.org/10.1021/acsenergylett.5c01642
ACS Energy Lett. 2025, 10, 4324−4331

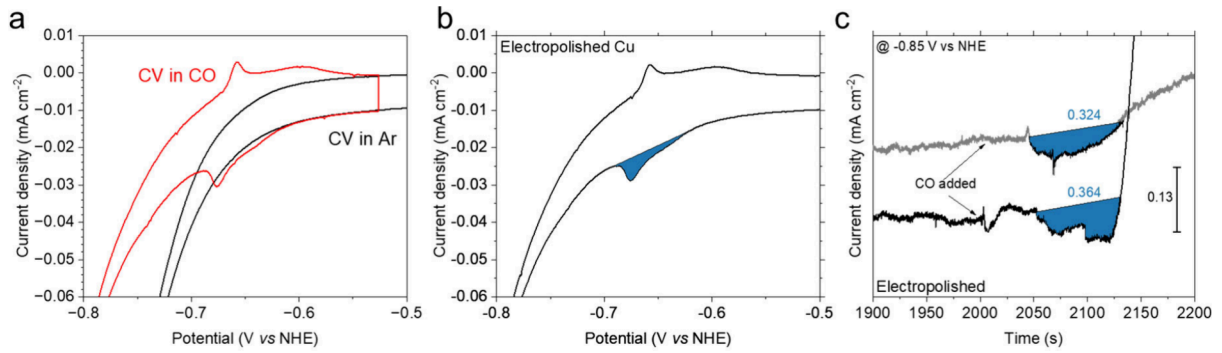

Figure 3. (a) Comparison of CVs for the electropolished copper foil in CO and Ar; (b) CO displacement CV of the electropolished Cu foil with the peak highlighted in the blue fill. The baseline of the peak was manually fitted by using the Origin software. Please see Supporting Information for further details of the peak area integration. CVs in (a) and (b) were conducted with the scan rate of 50 mV s^{-1} at 10 °C in pH 6.8 KH_2PO_4 phosphate buffer (0.1 M K_2HPO_4 + 0.1 M KH_2PO_4) with CO or Ar purged. CVs with different circle number were chosen and presented in both plots; (c) Chronoamperometry curves of the potential hold measurements at −0.85 V vs NHE in pH 6.8 phosphate buffer (0.1 M K_2HPO_4 + 0.1 M KH_2PO_4) on the electropolished copper foil and repeated on different electrodes.

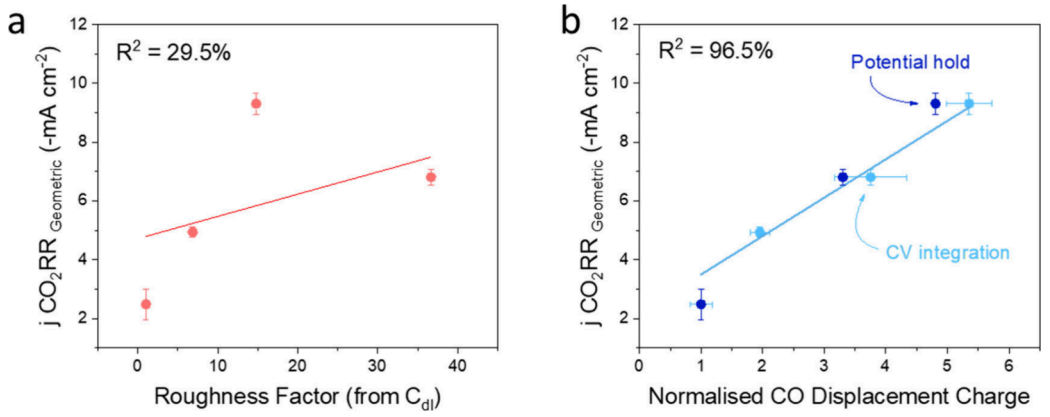

Figure 4. Relationships between the CO_2 reduction partial current densities normalized to geometric surface area (measured in 0.1 M $KHCO_3$, at −1.0 V vs RHE, and in H-cell) and (a) roughness factor measured by double layer capacitance (red), (b) normalised CO displacement charge measured by CV (light blue), and potential hold (dark blue). Error bars were calculated by repeating both the CO displacement reaction and CO_2RR for different electrodes and comparing the active surface area normalized current density towards CO_2RR.

S8). All potential hold experiments were performed at −0.85 V vs NHE, which was more negative than the displacement peak positions from Hori's single crystal studies (Figure S3)[43,59] and our own CV experiments (Figure S8). The initial current spike after the introduction of the CO was caused by the displacement with phosphate ions. Thereafter, the current decreases as the CO poisons the surface and diminishes the current due to H_2 evolution. However, a different magnitude of the CO poisoning effect to the HER current was observed in the repeating experiment shown by Figure 3a. As the HER behaviour of Cu with the presence of CO is complicated process[70] and beyond the scope of this paper, brief explanations on such feature can be found in SI. Potential hold also allows roughness factor comparisons between the current difference after CO introduction (Figures 3c and S8) and the integrated CV peak (Figures 3 and S8). The potential for hold was lower than the onset for the CORR, as shown by the electrochemistry mass spectrometry measurement (Figure S12).

The electropolished polycrystalline Cu was chosen as the reference and hence have a double layer capacitance roughness factor (RF) and normalized CO displacement charge of 1. The cathodic CO displacement peak area (Figure S8) of the nanostructured Cu was compared with that of the electropolished Cu to calculate the normalised CO displacement charge. The 3rd cycle of each CV scan was integrated, with the baseline of the slope corrected (Figure S13). The increase in current with the introduction of CO in the transient current curve (Figures 3c and S8) was also integrated and compared to the value for electropolished Cu to gauge further comparisons. The double layer capacitance was taken by cycling at various scan rates around 0 V *vs* the RHE in 0.1 M $HClO_4$ (Figure S14). The change in discharge current with increasing scan rates for the different electrodes were compared to electropolished Cu to form the roughness factor.

As mentioned, the normalized CO displacement charge and RF for the nanostructured electrodes were calculated against the electropolished electrode (CV integration, light blue, and potential hold, dark blue in Figures 4 and S15). The resulting raw values can be found in Table S1 and plotted in Figures 4 and S15. The nanostructured electrodes were tested toward the CO_2RR with an H-cell configuration in 0.1 M $KHCO_3$ electrolyte at −1.0 V vs RHE for an hour per potential.

As shown by Figure 4a, for the double layer capacitance RF vs the geometric CO_2RR current density, there is an absence of a linear relationship. Conversely, the normalized CO displace-

https://doi.org/10.1021/acsenergylett.5c01642
ACS Energy Lett. 2025, 10, 4324−4331

ment charge (Figure 4b) follows a linear relationship, well fitted vs the geometric CO_2RR current density. Another way of illustrating this is through plotting the active surface area normalized current density toward CO_2RR for CO displacement (CV integration, light blue, and potential hold, dark blue) and double layer capacitance (red) vs the nanostructured electrodes. In this case, a similar value indicates a similar estimated intrinsic activity towards CO_2RR of all different pretreated Cu-electrodes (Figure S15c). The double layer capacitance significantly overestimates the number of CO_2RR active sites in this work. The CO displacement, however, neatly normalizes the CO_2RR current density to the active surface area and deduces that increasing surface roughness through different methods does not improve the intrinsic activity. We propose that both CV integration (Figures 3a and S8a−d) and potential hold measurements (Figures 3b and S8e−h) are required for a more accurate CO_2RR active sites measurement due to the errors in integrating the CV with a broad peak and likewise, the errors in integrating the transient current increase for electrodes with lower CO_2RR active sites (Figure 3b). However, as no current active sites or ECSA quantification methods are absolute, in case of these two methods differ, we recommend cross comparing them with the results obtained from other characterization methods, like Pb-UPD, BET, CO-temperature-programmed deposition, and even the morphology analysis from electron microscopies, and consider the other properties of the Cu-based materials synthesized, to make appropriate selections.

The geometric and CO displacement active surface area normalized current densities are compared to other literature values normalized to double layer capacitance, with data adapted from Nitopi et al. (Figure S16).[71] The current density normalized by CO displacement active surface area for the pretreated electrodes converge to a greater extent at a higher partial current density than any other literature values. The above results also show that increasing the surface roughness does not improve the activity. Targeting surface roughness primarily affects the reaction selectivity by increasing the number of active sites without enhancing the intrinsic activity of each site. As surface roughness increases, so does the partial current density for oxygenated products, suppressing C_1 products on the electrode vs C_2 (Figure S17b). Surface roughness has two possible effects (i) increasing the number of strong binding undercoordinated sites[72,73] and (ii) effecting changes in mass transport of reactants and pH gradients.[74−76] It is therefore vital to accurately account for the active sites, not only to gauge the intrinsic activity of novel electrodes but also to accurately elucidate and model the effect of other surface changes on selectivity.

Our findings strongly suggest that closely packed (111) surfaces are inactive on nanostructured Cu surfaces, analogous to earlier studies on Cu single crystals:[57,77−80] we hence confirm the notion that findings on model extended surfaces can be translated to industrially relevant rough/high surface area Cu.

To conclude, this paper highlights the importance of accurate CO_2RR active sites measurements for the progression of material design, as research aims to improve the intrinsic activity of Cu and create novel materials towards CO_2RR. By comparing the CO_2RR current densities of 4 different nanostructured Cu electrodes normalized by double layer capacitance and CO displacement charge, we have shown CO displacement has distinct advantages over the widely used double layer capacitance method. To incorporate the method widely into the field, we currently recommend always benchmarking against electropolished Cu in pH 6.8 buffer at 10°C to gain a clear integration peak and reduce the error of the measurement. Future studies should focus on how variations in the CO displacement temperature, electrolyte pH, Cu working electrode potentials during the CO_2RR, and exposed Cu facets affect the accuracy of active sites quantification. Furthermore, it is imperative that the (or a) method is developed to allow the measurement of CO_2RR activity sites in industrially relevant single cells, such as membrane electrode assemblies, before, during, and after CO_2RR operation.

■ ASSOCIATED CONTENT

Supporting Information

The Supporting Information is available free of charge at https://pubs.acs.org/doi/10.1021/acsenergylett.5c01642.

Experimental and data analysis details, data in table format, and additional plots (PDF)

■ AUTHOR INFORMATION

Corresponding Authors

Ifan E. L. Stephens − *Department of Materials, Imperial College London, London SW7 2AZ, United Kingdom;* orcid.org/0000-0003-2157-492X; Email: i.stephens@imperial.ac.uk

Mary P. Ryan − *Department of Materials, Imperial College London, London SW7 2AZ, United Kingdom;* orcid.org/0000-0001-8582-3003; Email: m.p.ryan@imperial.ac.uk

Ludmilla Steier − *Department of Chemistry, Oxford University, Oxford OX1 3TA, United Kingdom;* Email: ludmilla.steier@chem.ox.ac.uk

Authors

Yuxiang Zhou − *Department of Materials, Imperial College London, London SW7 2AZ, United Kingdom*

Benjamin Bowers − *Department of Materials, Imperial College London, London SW7 2AZ, United Kingdom*

Alexander Bagger − *Department of Physics, Technical University of Denmark, Kongens Lyngby 2800, Denmark;* orcid.org/0000-0002-6394-029X

Guangmeimei Yang − *Department of Chemistry, Imperial College London, Molecular Sciences Research Hub, W12 0BZ London, United Kingdom;* orcid.org/0000-0002-8623-024X

Complete contact information is available at: https://pubs.acs.org/10.1021/acsenergylett.5c01642

Author Contributions

#Y.Z. and B.B. contributed equally to this work. These authors are co-first authors.

Notes

The authors declare no competing financial interest.

■ ACKNOWLEDGMENTS

B.B. thanks UKRI EPSRC (EP/2445673) for the funding. G.Y. thanks Imperial College London for the President's scholarship. A.B. acknowledges support from the Novo Nordisk Foundation Start Package Grant (Grant Number NNF23OC0084996) and the Pioneer Center for Accelerating P2X Materials Discovery (CAPeX), DNRF Grant Number P3.

L.S. thanks the Imperial College Research Fellowship and the Royal Society. We thank the help from Dr. Andreas Kafizas for the GIXRD measurement. We also acknowledge the support from Paula Sebastian Pascual for advice on the electropolishing method for polycrystalline Cu.

REFERENCES

(1) Bagger, A.; Ju, W.; Varela, A. S.; Strasser, P.; Rossmeisl, J. Electrochemical CO2 reduction: a classification problem. *ChemPhysChem* **2017**, *18* (22), 3266−3273.
(2) Corral, D.; Lee, D. U.; Ehlinger, V. M.; Nitopi, S.; Avilés Acosta, J. E.; Wang, L.; King, A. J.; Feaster, J. T.; Lin, Y.-R.; Weber, A. Z.; et al. Bridging knowledge gaps in liquid- and vapor-fed CO2 electrolysis through active electrode area. *Chem. Catalysis* **2022**, *2* (11), 3239−3253.
(3) Jia, F.; Yu, X.; Zhang, L. Enhanced selectivity for the electrochemical reduction of CO2 to alcohols in aqueous solution with nanostructured Cu−Au alloy as catalyst. *J. Power Sources* **2014**, *252*, 85−89.
(4) Kanase, R. S.; Lee, K. B.; Arunachalam, M.; Sivasankaran, R. P.; Oh, J.; Kang, S. H. Nanostructure engineering of Cu electrocatalyst for the selective C2+ hydrocarbons in electrochemical CO2 reduction. *Applied Surface Science* **2022**, *584*, No. 152518.
(5) Zhou, B.; Li, Q.; Zhang, Q.; Duan, J.; Jin, W. Sharply promoted CO2 diffusion in a mixed matrix membrane with hierarchical supra-nanostructured porous coordination polymer filler. *Journal of Membrane Science* **2020**, *597*, No. 117772.
(6) Zhang, T.; Li, Z.; Zhang, J.; Wu, J. Enhance CO2-to-C2+ products yield through spatial management of CO transport in Cu/ZnO tandem electrodes. *Journal of Catalysis* **2020**, *387*, 163−169.
(7) Song, Y.; Peng, R.; Hensley, D. K.; Bonnesen, P. V.; Liang, L.; Wu, Z.; Meyer, H. M.; Chi, M.; Ma, C.; Sumpter, B. G.; Rondinone, A. J. High-Selectivity Electrochemical Conversion of CO_2 to Ethanol Using a Copper Nanoparticle/N-Doped Graphene Electrode. *ChemistrySelect* **2016**, *1* (19), 6055−6061.
(8) Morales-Guio, C. G.; Cave, E. R.; Nitopi, S. A.; Feaster, J. T.; Wang, L.; Kuhl, K. P.; Jackson, A.; Johnson, N. C.; Abram, D. N.; Hatsukade, T.; et al. Improved CO2 reduction activity towards C2+ alcohols on a tandem gold on copper electrocatalyst. *Nature Catalysis* **2018**, *1* (10), 764−771.
(9) Zhu, Y.; Cui, X.; Liu, H.; Guo, Z.; Dang, Y.; Fan, Z.; Zhang, Z.; Hu, W. Tandem catalysis in electrochemical CO2 reduction reaction. *Nano Research* **2021**, *14*, 4471−4486.
(10) She, X.; Zhang, T.; Li, Z.; Li, H.; Xu, H.; Wu, J. Tandem Electrodes for Carbon Dioxide Reduction into C2+ Products at Simultaneously High Production Efficiency and Rate. *Cell Reports Physical Science* **2020**, *1* (4), No. 100051.
(11) Varela, A. S.; Schlaup, C.; Jovanov, Z. P.; Malacrida, P.; Horch, S.; Stephens, I. E. L.; Chorkendorff, I. CO2 Electroreduction on Well-Defined Bimetallic Surfaces: Cu Overlayers on Pt(111) and Pt(211). *J. Phys. Chem. C* **2013**, *117*, 20500−20508.
(12) Lu, L.; Sun, X.; Ma, J.; Yang, D.; Wu, H.; Zhang, B.; Zhang, J.; Han, B. Highly Efficient Electroreduction of CO2 to Methanol on Palladium−Copper Bimetallic Aerogels. *Angew. Chem., Int. Ed.* **2018**, *57* (43), 14149−14153.
(13) Gao, D.; Arán-Ais, R. M.; Jeon, H. S.; Roldan Cuenya, B. Rational catalyst and electrolyte design for CO2 electroreduction towards multicarbon products. *Nature Catalysis* **2019**, *2* (3), 198−210.
(14) Kim, D.; Resasco, J.; Yu, Y.; Asiri, A. M.; Yang, P. Synergistic geometric and electronic effects for electrochemical reduction of carbon dioxide using gold−copper bimetallic nanoparticles. *Nat. Commun.* **2014**, *5* (1), 4948.
(15) Nishimura, Y. F.; Peng, H.-J.; Nitopi, S.; Bajdich, M.; Wang, L.; Morales-Guio, C. G.; Abild-Pedersen, F.; Jaramillo, T. F.; Hahn, C. Guiding the Catalytic Properties of Copper for Electrochemical CO2 Reduction by Metal Atom Decoration. *ACS Appl. Mater. Interfaces* **2021**, *13* (44), 52044−52054.
(16) van den Berg, D.; Brouwer, J. C.; Hendrikx, R. W.; Kortlever, R. Experimental screening of intermetallic alloys for electrochemical CO2 reduction. *Catalysis Today* **2024**, *439*, No. 114805.
(17) Sandberg, R. B.; Montoya, J. H.; Chan, K.; Nørskov, J. K. CO-CO coupling on Cu facets: Coverage, strain and field effects. *Surface Science* **2016**, *654*, 56−62.
(18) Zhu, C.; Zhang, Z.; Zhong, L.; Hsu, C.-S.; Xu, X.; Li, Y.; Zhao, S.; Chen, S.; Yu, J.; Chen, S.; et al. Product-Specific Active Site Motifs of Cu for Electrochemical CO2 Reduction. *Chem.* **2021**, *7* (2), 406−420.
(19) Moura de Salles Pupo, M.; Kortlever, R. Electrolyte Effects on the Electrochemical Reduction of CO2. *ChemPhysChem* **2019**, *20* (22), 2926−2935.
(20) Marcandalli, G.; Goyal, A.; Koper, M. T. M. Electrolyte Effects on the Faradaic Efficiency of CO2 Reduction to CO on a Gold Electrode. *ACS Catal.* **2021**, *11* (9), 4936−4945.
(21) Monteiro, M. C. O.; Dattila, F.; Hagedoorn, B.; García-Muelas, R.; López, N.; Koper, M. T. M. Absence of CO2 electroreduction on copper, gold and silver electrodes without metal cations in solution. *Nature Catalysis* **2021**, *4* (8), 654−662.
(22) Yoo, S.; Park, S.; Son, J.; Kim, J.; Shin, H.; Hwang, Y. J. Excess Cations Alter* CO Intermediate Configuration and Product Selectivity of Cu in Acidic Electrochemical CO2 Reduction Reaction. *J. Am. Chem. Soc.* **2025**, *147* (15), 12996−13007.
(23) Lee, S. Y.; Kim, J.; Bak, G.; Lee, E.; Kim, D.; Yoo, S.; Kim, J.; Yun, H.; Hwang, Y. J. Probing cation effects on* CO intermediates from electroreduction of CO2 through operando Raman spectroscopy. *J. Am. Chem. Soc.* **2023**, *145* (42), 23068−23075.
(24) Burgers, I.; Wortmann, B.; Garcia, A. C.; Deacon-Price, C.; Pérez-Gallent, E.; Goetheer, E.; Kortlever, R. The Effect of Salts on the CO2 Reduction Product Distribution in an Aprotic Electrolyte. *ChemPhysChem* **2024**, *25* (24), No. e202400589.
(25) Chen, X.; Chen, J.; Alghoraibi, N. M.; Henckel, D. A.; Zhang, R.; Nwabara, U. O.; Madsen, K. E.; Kenis, P. J. A.; Zimmerman, S. C.; Gewirth, A. A. Electrochemical CO2-to-ethylene conversion on polyamine-incorporated Cu electrodes. *Nature Catalysis* **2021**, *4* (1), 20−27.
(26) Wang, X.; Wang, Z.; García de Arquer, F. P.; Dinh, C.-T.; Ozden, A.; Li, Y. C.; Nam, D.-H.; Li, J.; Liu, Y.-S.; Wicks, J.; et al. Efficient electrically powered CO2-to-ethanol via suppression of deoxygenation. *Nature Energy* **2020**, *5* (6), 478−486.
(27) Kuhl, K. P.; Cave, E. R.; Abram, D. N.; Jaramillo, T. F. New insights into the electrochemical reduction of carbon dioxide on metallic copper surfaces. *Energy Environ. Sci.* **2012**, *5* (5), 7050−7059.
(28) Hori, Y.; Kikuchi, K.; Murata, A.; Suzuki, S. Production of Methane and Ethylene in Electrochemical Reduction of Carbon Dioxide at Copper Electrode in Aqueous Hydrogencarbonate Solution. *Chemistry Letters* **1986**, *15* (6), 897−898.
(29) Chan, K. A Few Basic Concepts In Electrochemical Carbon Dioxide Reduction. *Nat. Commun.* **2020**, *11* (1), 5954.
(30) Amirbeigiarab, R.; Tian, J.; Herzog, A.; Qiu, C.; Bergmann, A.; Roldan Cuenya, B.; Magnussen, O. M. Atomic-scale surface restructuring of copper electrodes under CO2 electroreduction conditions. *Nature Catalysis* **2023**, *6* (9), 837−846.
(31) Lee, S. H.; Lin, J. C.; Farmand, M.; Landers, A. T.; Feaster, J. T.; Avilés Acosta, J. E.; Beeman, J. W.; Ye, Y.; Yano, J.; Mehta, A.; et al. Oxidation State and Surface Reconstruction of Cu under CO2 Reduction Conditions from In Situ X-ray Characterization. *J. Am. Chem. Soc.* **2021**, *143* (2), 588−592.
(32) Mom, R. V.; Sandoval-Diaz, L.-E.; Gao, D.; Chuang, C.-H.; Carbonio, E. A.; Jones, T. E.; Arrigo, R.; Ivanov, D.; Hävecker, M.; Roldan Cuenya, B.; et al. Assessment of the Degradation Mechanisms of Cu Electrodes during the CO2 Reduction Reaction. *ACS Appl. Mater. Interfaces* **2023**, *15* (25), 30052−30059.
(33) Vavra, J.; Ramona, G. P. L.; Dattila, F.; Kormányos, A.; Priamushko, T.; Albertini, P. P.; Loiudice, A.; Cherevko, S.; Lopéz, N.; Buonsanti, R. Solution-based Cu+ transient species mediate the reconstruction of copper electrocatalysts for CO2 reduction. *Nature Catalysis* **2024**, *7*, 89.

https://doi.org/10.1021/acsenergylett.5c01642
ACS Energy Lett. 2025, 10, 4324−4331

(34) Okatenko, V.; Loiudice, A.; Newton, M. A.; Stoian, D. C.; Blokhina, A.; Chen, A. N.; Rossi, K.; Buonsanti, R. Alloying as a Strategy to Boost the Stability of Copper Nanocatalysts during the Electrochemical CO2 Reduction Reaction. *J. Am. Chem. Soc.* **2023**, *145* (9), 5370−5383.
(35) Grosse, P.; Yoon, A.; Rettenmaier, C.; Herzog, A.; Chee, S. W.; Roldan Cuenya, B. Dynamic transformation of cubic copper catalysts during CO2 electroreduction and its impact on catalytic selectivity. *Nat. Commun.* **2021**, *12* (1), 6736.
(36) Choi, W.; Won, D. H.; Hwang, Y. J. Catalyst design strategies for stable electrochemical CO2 reduction reaction. *Journal of Materials Chemistry A* **2020**, *8* (31), 15341−15357.
(37) Röttcher, N. C.; Ku, Y.-P.; Minichova, M.; Ehelebe, K.; Cherevko, S. Comparison of methods to determine electrocatalysts' surface area in gas diffusion electrode setups: a case study on Pt/C and PtRu/C. *Journal of Physics: Energy* **2023**, *5* (2), No. 024007.
(38) Verdaguer-Casadevall, A.; Li, C. W.; Johansson, T. P.; Scott, S. B.; McKeown, J. T.; Kumar, M.; Stephens, I. E. L.; Kanan, M. W.; Chorkendorff, I. Probing the Active Surface Sites for CO Reduction on Oxide-Derived Copper Electrocatalysts. *J. Am. Chem. Soc.* **2015**, *137* (31), 9808−9811.
(39) Chen, D.; Tao, Q.; Liao, L. W.; Liu, S. X.; Chen, Y. X.; Ye, S. Determining the Active Surface Area for Various Platinum Electrodes. *Electrocatalysis* **2011**, *2* (3), 207−219.
(40) Wu, J. Understanding the Electric Double-Layer Structure, Capacitance, and Charging Dynamics. *Chem. Rev.* **2022**, *122* (12), 10821−10859.
(41) Wei, C.; Rao, R. R.; Peng, J.; Huang, B.; Stephens, I. E. L.; Risch, M.; Xu, Z. J.; Shao-Horn, Y. Recommended Practices and Benchmark Activity for Hydrogen and Oxygen Electrocatalysis in Water Splitting and Fuel Cells. *Advanced Materials* **2019**, *31* (31), No. 1806296.
(42) Jeon, S. S.; Kang, P. W.; Klingenhof, M.; Lee, H.; Dionigi, F.; Strasser, P. Active Surface Area and Intrinsic Catalytic Oxygen Evolution Reactivity of NiFe LDH at Reactive Electrode Potentials Using Capacitances. *ACS Catal.* **2023**, *13* (2), 1186−1196.
(43) Hori, Y.; Wakebe, H.; Tsukamoto, T.; Koga, O. Adsorption of CO accompanied with simultaneous charge transfer on copper single crystal electrodes related with electrochemical reduction of CO2 to hydrocarbons. *Surface Science* **1995**, *335*, 258−263.
(44) Hori, Y.; Murata, A.; Tsukamoto, T.; Wakebe, H.; Koga, O.; Yamazaki, H. Adsoprtion of carbon monoxide at a copper electrode accompanied by electron transfer observed by voltammetry and IR spectroscopy. *Electrochimica Acta* **1994**, *39* (17), 2495−2500.
(45) Koga, O.; Watanabe, Y.; Tanizaki, M.; Hori, Y. Specific adsorption of anions on a copper (100) single crystal electrode studied by charge displacement by CO adsorption and infrared spectroscopy. *Electrochimica Acta* **2001**, *46* (20), 3083−3090.
(46) Sebastián-Pascual, P.; Petersen, A. S.; Bagger, A.; Rossmeisl, J.; Escudero-Escribano, M. pH and Anion Effects on Cu−Phosphate Interfaces for CO Electroreduction. *ACS Catal.* **2021**, *11* (3), 1128−1135.
(47) Peterson, A. A.; Nørskov, J. K. Activity descriptors for CO2 electroreduction to methane on transition-metal catalysts. *J. Phys. Chem. Lett.* **2012**, *3* (2), 251−258.
(48) Kuhl, K. P.; Hatsukade, T.; Cave, E. R.; Abram, D. N.; Kibsgaard, J.; Jaramillo, T. F. Electrocatalytic conversion of carbon dioxide to methane and methanol on transition metal surfaces. *J. Am. Chem. Soc.* **2014**, *136* (40), 14107−14113.
(49) Su, J.; Yu, L.; Han, B.; Li, F.; Chen, Z.; Zeng, X. C. Enhanced CO_2 reduction on a Cu-decorated single-atom catalyst via an inverse sandwich M-Graphene-Cu structure. *J. Phys. Chem. Lett.* **2024**, *15* (33), 8600−8607.
(50) Chauhan, P.; Georgi, M.; Herranz, J.; Müller, G.; Diercks, J. S.; Eychmüller, A.; Schmidt, T. J. Impact of Surface Composition Changes on the CO2-Reduction Performance of Au−Cu Aerogels. *Langmuir* **2024**, *40* (23), 12288−12300.
(51) Nie, X.; Esopi, M. R.; Janik, M. J.; Asthagiri, A. Selectivity of CO_2 Reduction on Copper Electrodes: The Role of the Kinetics of Elementary Steps. *Angew. Chem., Int. Ed.* **2013**, *52* (9), 2459.
(52) Hori, Y.; Takahashi, I.; Koga, O.; Hoshi, N. Electrochemical reduction of carbon dioxide at various series of copper single crystal electrodes. *J. Mol. Catal. A: Chem.* **2003**, *199* (1), 39−47.
(53) Hori, Y.; Murata, A.; Takahashi, R. Formation of hydrocarbons in the electrochemical reduction of carbon dioxide at a copper electrode in aqueous solution. *Journal of the Chemical Society, Faraday Transactions 1: Physical Chemistry in Condensed Phases* **1989**, *85* (8), 2309−2326.
(54) Bagger, A.; Ju, W.; Varela, A. S.; Strasser, P.; Rossmeisl, J. Single site porphyrine-like structures advantages over metals for selective electrochemical CO2 reduction. *Catalysis Today* **2017**, *288*, 74−78.
(55) Bagger, A.; Ju, W.; Varela, A. S.; Strasser, P.; Rossmeisl, J. Electrochemical CO2 Reduction: Classifying Cu Facets. *ACS Catal.* **2019**, *9* (9), 7894−7899.
(56) Engstfeld, A. K.; Maagaard, T.; Horch, S.; Chorkendorff, I.; Stephens, I. E. L. Polycrystalline and Single-Crystal Cu Electrodes: Influence of Experimental Conditions on the Electrochemical Properties in Alkaline Media. *Chemistry − A European Journal* **2018**, *24* (67), 17743−17755.
(57) Cheng, D.; Nguyen, K.-L. C.; Sumaria, V.; Wei, Z.; Zhang, Z.; Gee, W.; Li, Y.; Morales-Guio, C. G.; Heyde, M.; Roldan Cuenya, B.; et al. Structure sensitivity and catalyst restructuring for CO2 electroreduction on copper. *Nat. Commun.* **2025**, *16* (1), 4064.
(58) Tiwari, A.; Heenen, H. H.; Bjørnlund, A. S.; Maagaard, T.; Cho, E.; Chorkendorff, I.; Kristoffersen, H. H.; Chan, K.; Horch, S. Fingerprint Voltammograms of Copper Single Crystals under Alkaline Conditions: A Fundamental Mechanistic Analysis. *J. Phys. Chem. Lett.* **2020**, *11* (4), 1450−1455.
(59) Koga, O.; Teruya, S.; Matsuda, K.; Minami, M.; Hoshi, N.; Hori, Y. Infrared spectroscopic and voltammetric study of adsorbed CO on stepped surfaces of copper monocrystalline electrodes. *Electrochimica Acta* **2005**, *50* (12), 2475−2485.
(60) Hochfilzer, D.; Tiwari, A.; Clark, E. L.; Bjørnlund, A. S.; Maagaard, T.; Horch, S.; Seger, B.; Chorkendorff, I.; Kibsgaard, J. In Situ Analysis of the Facets of Cu-Based Electrocatalysts in Alkaline Media Using Pb Underpotential Deposition. *Langmuir* **2022**, *38* (4), 1514−1521.
(61) Raaijman, S. J.; Arulmozhi, N.; Koper, M. T. M. Morphological Stability of Copper Surfaces under Reducing Conditions. *ACS Appl. Mater. Interfaces* **2021**, *13* (41), 48730−48744.
(62) P. Schouten, K. J.; Gallent, E. P.; Koper, M. T. M. The electrochemical characterization of copper single-crystal electrodes in alkaline media. *Journal of Electroanalytical Chemistry* **2013**, *699*, 6−9.
(63) Le Duff, C. S.; Lawrence, M. J.; Rodriguez, P. Role of the Adsorbed Oxygen Species in the Selective Electrochemical Reduction of CO2 to Alcohols and Carbonyls on Copper Electrodes. *Angew. Chem., Int. Ed.* **2017**, *56* (42), 12919−12924.
(64) Xue, S.; Garlyyev, B.; Auer, A.; Kunze-Liebhäuser, J.; Bandarenka, A. S. How the Nature of the Alkali Metal Cations Influences the Double-Layer Capacitance of Cu, Au, and Pt Single-Crystal Electrodes. *J. Phys. Chem. C* **2020**, *124* (23), 12442−12447.
(65) Hori, Y.; Wakebe, H.; Tsukamoto, T.; Koga, O. Electrocatalytic process of CO selectivity in electrochemical reduction of CO2 at metal electrodes in aqueous media. *Electrochimica Acta* **1994**, *39* (11), 1833−1839.
(66) Luo, J.; Steier, L.; Son, M.-K.; Schreier, M.; Mayer, M. T.; Grätzel, M. Cu2O Nanowire Photocathodes for Efficient and Durable Solar Water Splitting. *Nano Lett.* **2016**, *16* (3), 1848−1857.
(67) Schreier, M.; Héroguel, F.; Steier, L.; Ahmad, S.; Luterbacher, J. S.; Mayer, M. T.; Luo, J.; Grätzel, M. Solar conversion of CO2 to CO using Earth-abundant electrocatalysts prepared by atomic layer modification of CuO. *Nature Energy* **2017**, *2* (7), No. 17087.
(68) Giri, S. D.; Sarkar, A. Electrochemical Study of Bulk and Monolayer Copper in Alkaline Solution. *J. Electrochem. Soc.* **2016**, *163* (3), H252.

https://doi.org/10.1021/acsenergylett.5c01642
ACS Energy Lett. 2025, 10, 4324−4331

(69) Kas, R.; Kortlever, R.; Milbrat, A.; Koper, M. T. M.; Mul, G.; Baltrusaitis, J. Electrochemical CO2 reduction on Cu2O-derived copper nanoparticles: controlling the catalytic selectivity of hydrocarbons. *Physical Chemistry Chemical Physics* **2014**, *16* (24), 12194−12201.
(70) Zhang, Y.-J.; Sethuraman, V.; Michalsky, R.; Peterson, A. A. Competition between CO2 reduction and H2 evolution on transition-metal electrocatalysts. *ACS Catal.* **2014**, *4* (10), 3742−3748.
(71) Nitopi, S.; Bertheussen, E.; Scott, S. B.; Liu, X. Y.; Engstfeld, A. K.; Horch, S.; Seger, B.; Stephens, I. E. L.; Chan, K.; Hahn, C.; et al. Progress and Perspectives of Electrochemical CO2 Reduction on Copper in Aqueous Electrolyte. *Chem. Rev.* **2019**, *119* (12), 7610−7672.
(72) Bagger, A.; Ju, W.; Varela, A. S.; Strasser, P.; Rossmeisl, J. Electrochemical CO_2 reduction: classifying Cu facets. *ACS Catal.* **2019**, *9* (9), 7894−7899.
(73) Verdaguer-Casadevall, A.; Li, C. W.; Johansson, T. P.; Scott, S. B.; McKeown, J. T.; Kumar, M.; Stephens, I. E.; Kanan, M. W.; Chorkendorff, I. Probing the active surface sites for CO reduction on oxide-derived copper electrocatalysts. *J. Am. Chem. Soc.* **2015**, *137* (31), 9808−9811.
(74) Raciti, D.; Mao, M.; Wang, C. Mass transport modelling for the electroreduction of CO2 on Cu nanowires. *Nanotechnology* **2018**, *29* (4), No. 044001.
(75) Wang, L.; Nitopi, S.; Wong, A. B.; Snider, J. L.; Nielander, A. C.; Morales-Guio, C. G.; Orazov, M.; Higgins, D. C.; Hahn, C.; Jaramillo, T. F. Electrochemically converting carbon monoxide to liquid fuels by directing selectivity with electrode surface area. *Nature Catalysis* **2019**, *2* (8), 702−708.
(76) Dolmanan, S. B.; Böhme, A.; Fan, Z.; King, A. J.; Fenwick, A. Q.; Handoko, A. D.; Leow, W. R.; Weber, A. Z.; Ma, X.; Khoo, E.; et al. Local microenvironment tuning induces switching between electrochemical CO2 reduction pathways. *Journal of Materials Chemistry A* **2023**, *11* (25), 13493−13501.
(77) Schouten, K. J. P.; Pérez Gallent, E.; Koper, M. T. Structure sensitivity of the electrochemical reduction of carbon monoxide on copper single crystals. *ACS Catal.* **2013**, *3* (6), 1292−1295.
(78) Hori, Y.; Takahashi, I.; Koga, O.; Hoshi, N. Electrochemical reduction of carbon dioxide at various series of copper single crystal electrodes. *J. Mol. Catal. A: Chem.* **2003**, *199* (1-2), 39−47.
(79) Takahashi, I.; Koga, O.; Hoshi, N.; Hori, Y. Electrochemical reduction of CO2 at copper single crystal Cu (S)-[n (111)×(111)] and Cu (S)-[n (110)×(100)] electrodes. *Journal of Electroanalytical Chemistry* **2002**, *533* (1-2), 135−143.
(80) Liu, G.; Lee, M.; Kwon, S.; Zeng, G.; Eichhorn, J.; Buckley, A. K.; Toste, F. D.; Goddard III, W. A.; Toma, F. M. CO2 reduction on pure Cu produces only H2 after subsurface O is depleted: Theory and experiment. *Proc. Natl. Acad. Sci. U. S. A.* **2021**, *118* (23), No. e2012649118.

https://doi.org/10.1021/acsenergylett.5c01642
ACS Energy Lett. 2025, 10, 4324−4331